Electronic structure and luminescence of $[(CH_3)_4N]_2MnX_4$ (X=Cl,Br) crystals at high pressures by time-resolved spectroscopy: Pressure effects on the Mn-Mn exchange coupling

Y. Rodríguez-Lazcano,* L. Nataf, and F. Rodríguez
MALTA Consolider Team, DCITIMAC, Facultad de Ciencias, University of Cantabria, 39005 Santander, Spain
(Received 2 March 2009; revised manuscript received 6 July 2009; published 24 August 2009)

This work investigates the Mn^{2+} photoluminescence (PL) and electronic structure of $[(CH_3)_4N]_2MnX_4$ (X:Cl,Br) and their variation with pressure through time-resolved spectroscopy in the 0–15 GPa range. The crystal-field excitation and emission spectra are explained on the basis of the $MnX_4^{2-}(T_d)$ tetrahedra. Their peaks experience large pressure redshifts, which are associated with the big crystal compressibility and the interaction between organic/inorganic ($[CH_3]_4N^-/MnX_4^{2-}$) tetrahedra. The variation in the Racah parameters and crystal-field splitting with pressure indicates that the excitation and emission redshifts of Mn^{2+} are mainly governed by the increase in the Mn-X bond covalency (70%) rather than the increase in the crystal-field splitting (30%). Above 6 GPa, pressure induces structural modifications, which are related to aggregation of the MnX_4^{2-} tetrahedra with change in Mn^{2+} coordination from fourfold $MnX_4^{2-}(T_d)$ to sixfold $MnX_6^{4-}(O_h)$. This process involves a drastic change in the PL behavior yielding a simultaneous two-color PL emission: green emission at 520 nm and a red emission around 650 nm. Both emissions experience noticeable redshifts with pressure producing a marked piezo-PL effect. The large pressure range of phase coexistence makes these materials attractive for multiband PL, the wavelengths of which can be tuned through pressure and eventually stabilized at ambient conditions.

DOI: 10.1103/PhysRevB.80.085115 PACS number(s): 61.50.Ks, 71.70.−d, 78.55.−m, 81.40.Vw

I. INTRODUCTION

$[(CH_3)_4N]_2MnCl_4$ and $[(CH_3)_4N]_2MnBr_4$ are efficient photoluminescence (PL) compounds emitting green light (520 nm) from the photoexcited MnX_4^{2-} (X: Cl, Br) inorganic tetrahedra. These materials have received considerable attention for optical studies due to their capabilities as phosphors, sensors as well as their triboluminescence and piezochromic properties largely arising as consequence of the interactions between organic/inorganic tetrahedra.[1–10] Their intense green PL is fully related to the $^4T_1 \rightarrow {}^6A_1$ electronic transition of Mn^{2+} from MnX_4^{2-} tetrahedra, which appear isolated within the crystal.[1–3,7,8,11] The $Mn^{2+}(T_d)$ green PL contrasts with that attained in the analog trichlorides $(CH_3)_4NMnX_3$ (X: Cl, Br), whose inorganic $MnCl_3^-$ anions are coupled, forming linear chains of face-sharing octahedra (Figs. 1 and 2). The sixfold coordinate D_{3d} (nearly O_h) Mn^{2+} is responsible for the intense red PL around 630 nm exhibited by this crystal at ambient conditions. The absence of center of inversion in $MnX_4^{2-}(T_d)$ and the small crystal-field splitting between e-t_2 3d-Mn^{2+} orbitals, Δ=0.4 eV, increase the electric-dipole oscillator strength of Mn^{2+} transitions, yielding an intense green PL in $[(CH_3)_4N]_2MnX_4$. On the other hand, the MnX_3Mn exchange interaction between nearest Mn^{2+} along the linear chains in $(CH_3)_4NMnX_3$ together with the larger crystal-field splitting, Δ=0.8 eV, are responsible for the enhanced absorption of the sixfold centrosymmetric Mn^{2+} and hence its intense red PL (Fig. 3). In both compounds, the absorption coefficient of the crystal-field peaks in bromides is an order of magnitude larger than the corresponding Mn^{2+} absorption coefficient in chlorides[7–13] such as is illustrated in Figs. 1 and 2 and Table I.

Despite Mn^{2+} absorption enhancement in these compounds, the oscillator strength of their crystal-field transitions is however very weak ($f \sim 10^{-5}$) leading to weak absorption peaks in comparison to other transition metal compounds.[14,15,18] In $[(CH_3)_4N]_2MnBr_4$ the most intense crystal-field peak ($^4A_1$ ^4E) has an optical density smaller than 0.02 for sample thickness of 20 μm,[19] a limitation which is crucial to perform high-pressure absorption measurements, in diamond anvil cells (DAC). Therefore, in order to achieve the goal of studying pressure variations in crystal-field spectra in $Mn^{2+}(T_d)$, we used high-pressure time-resolved excitation spectroscopy. This technique enables us to obtain precise excitation spectra at high pressure thus providing pioneering results on the energy variation in the crystal-field states of MnX_4^{2-} (X: Cl,Br) with pressure.

It is worth noting that the intense $Mn^{2+}(T_d)$ green emission in $[(CH_3)_4N]_2MnX_4$ is somehow subtle as can be modified by slight changes in the crystal volume and temperature.[1–4] In fact the PL quantum yield, which is near to 1 at ambient conditions, drastically reduces by increasing temperature. In $[(C_4H_9)_4N]_2MnCl_4$, the PL drops an order of magnitude few degrees above room temperature and eventually quenches at T=345 K.[3] The PL quenching was related to de-excitation nonradiative phenomena caused by multiphonon (or multiroton) relaxation due to interactions between the $(C_4H_9)_4N^-$ and $MnCl_4^{2-}$ tetrahedra.[3] On the other hand, earlier investigations on the pressure behavior of $Mn^{2+}(T_d)$ PL in $[(C_2H_5)_4N]_2MnBr_4$ and $[pyH]_2MnCl_4$ in the 0–0.4 GPa range, reported large pressure-induced PL redshift: −32 and −25 meV/GPa, respectively.[4] Later experiments carried out in the doubly-red-green PL material $[(CH_3)_3NH]_3Mn_2Cl_7$ in the 0–1.2 GPa range showed that the red PL redshifted with pressure by −74 meV/GPa, which is six times larger than the green emission redshift of −12 meV/GPa,[20] and 70 times larger than the ruby R-lines widely employed as pressure gauge in high-pressure experiments.[21] Nevertheless the mechanism responsible for the large pressure shifts and their different rate remain unex-

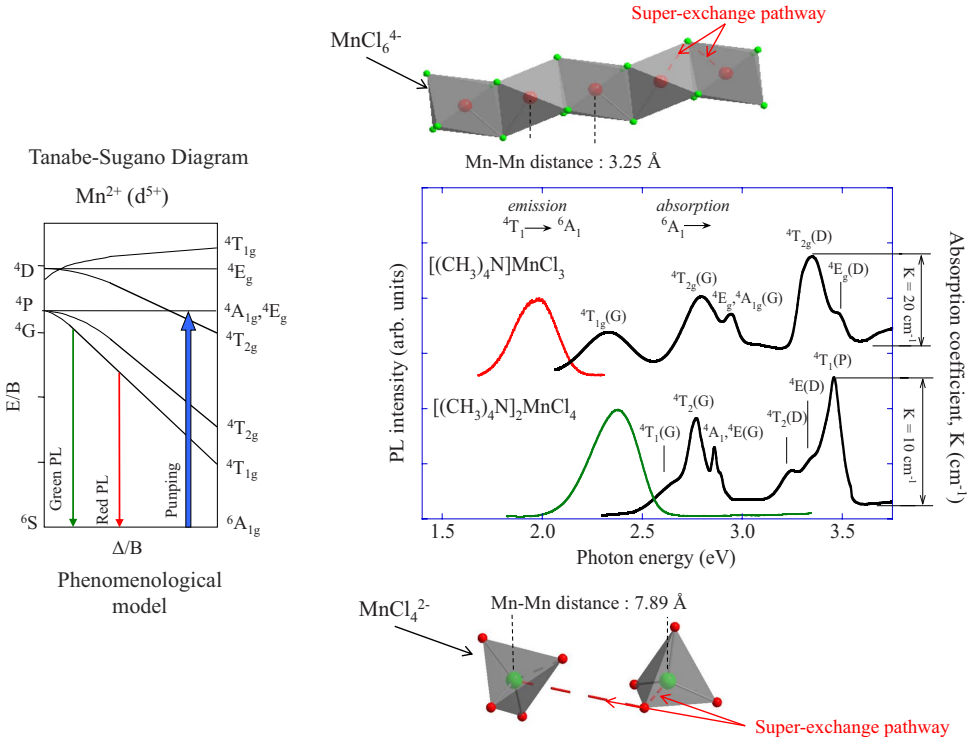

FIG. 1. (Color online) Absorption and corresponding emission spectra at ambient conditions of single crystals of $[(CH_3)_4N]_2MnCl_4$ and $(CH_3)_4NMnCl_3$. The peaks are assigned to crystal-field transitions of Mn^{2+} within the $MnX_4^{2-}(T_d)$ and $MnX_6^{4-}(O_h)$, respectively, and are labeled with corresponding excited state irreps. The schematic Tanabe-Sugano diagram for Mn^{2+} illustrates the origin of the different green and red emissions of each compound. A schematic representation of the hexagonal $P6_3/m$ structure of $(CH_3)_4NMnCl_3$ and the orthorhombic *Pmcn* crystal structure of $[(CH_3)_4N]_2MnCl_4$ are shown. The coordination polyhedron of Mn^{2+} and the super-exchange pathway are indicated in each structure.

plained. Furthermore the variation in the excitation spectra and associated lifetime with pressure as well as the PL behavior at higher pressures ($P>1$ GPa) in this highly efficient PL materials have not been explored yet. Recent findings on fluorite-type crystals such as $(Ca,Sr,Ba)F_2:Mn^{2+}$ (Ref. 22) and rutile-type MnF_2 (Ref. 16) reveal the efficacy of pressure-induced structural changes to induce, or even create, PL phenomena in concentrated materials of transition metal ions, yielding more efficient PL phases with multiband emission.

The aim of this work is to correlate the variations in PL induced by pressure with the variations undergone by the corresponding crystal-field spectrum and associated PL lifetime of MnX_4^{2-} in $[(CH_3)_4N]_2MnX_4$ for X: Cl, Br. Our inter-

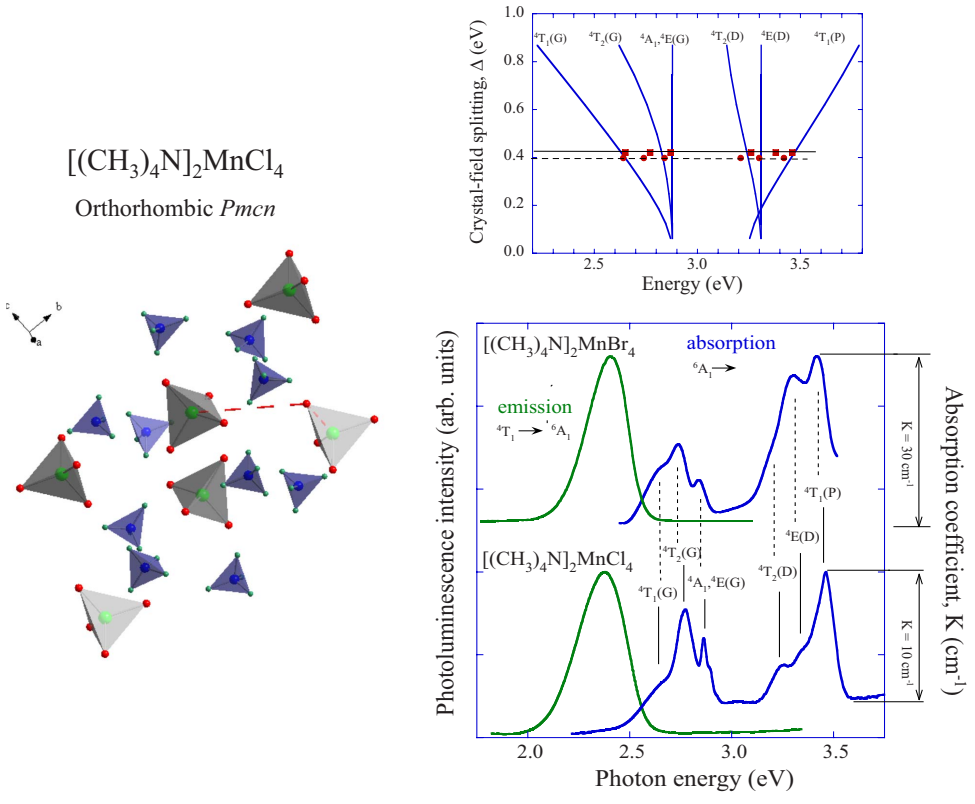

FIG. 2. (Color online) Absorption and emission spectra at ambient conditions of single crystals of $[(CH_3)_4N]_2MnCl_4$ and $[(CH_3)_4N]_2MnBr_4$. The peaks are assigned to crystal-field transitions of Mn^{2+} within the $MnX_4^{2-}(T_d)$ and are labeled with corresponding excited state irreps. The energy level diagram corresponds the calculated Tanabe-Sugano diagrams for $Mn^{2+}(T_d)$ as a function of the crystal-field parameter, Δ, for $B=0.078$ eV and $C=0.381$ eV ($C/B=4.88$). The experimental points correspond to the peak energy for $[(CH_3)_4N]_2MnCl_4$ (■) and $[(CH_3)_4N]_2MnBr_4$ (●). Symbols in parenthesis: (squares in red color) and (● in red color) in color (online). The *Pmcn* crystal structure of the compounds showing the organic $(CH_3)_4N^+$ and inorganic MnX_4^{2-} tetrahedra is shown.

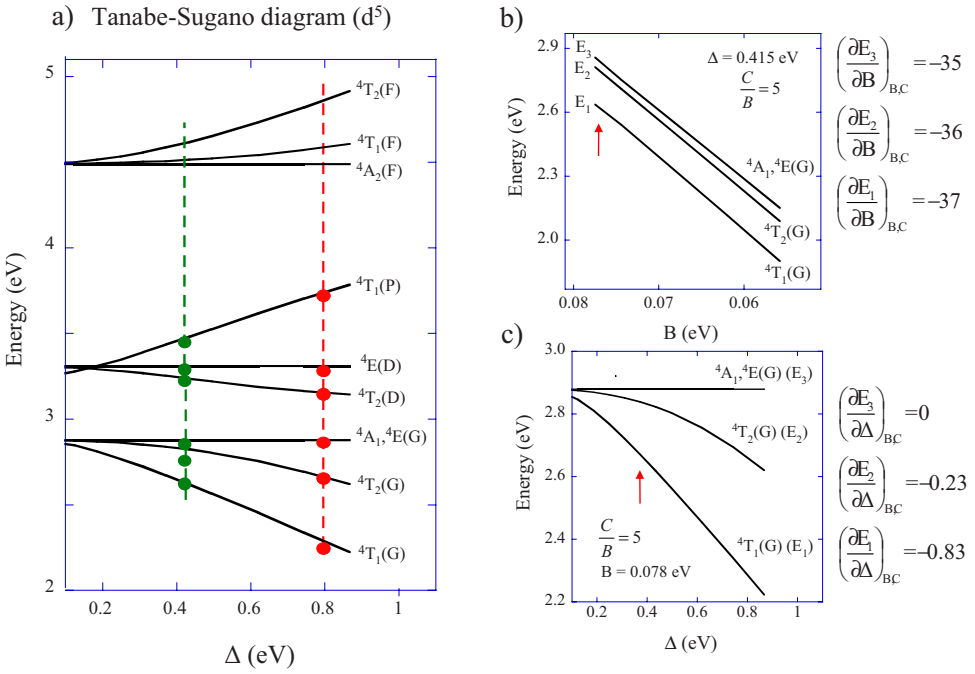

FIG. 3. (Color online) (a) Calculated Tanabe-Sugano diagrams for Mn^{2+} as a function of the crystal-field parameter, Δ, for $B=0.078$ eV and $C=0.39$ eV ($C/B=5$). The points represent the experimental data for $[(CH_3)_4N]_2MnCl_4$ (●) and $(CH_3)_4NMnCl_3$ (●) obtained from the corresponding optical absorption spectra. Symbols in parenthesis $[(CH_3)_4N]_2MnCl_4$ (● green) and $(CH_3)_4NMnCl_3$ (● red) in color (online). (b) Tanabe-Sugano diagram for Mn^{2+} as a function of the crystal-field splitting Δ, and (c) the Racah parameter B, for $C/B=4.9$. The red arrows represent the B- and Δ-points where $\frac{\partial E_i}{\partial \Delta}$ and $\frac{\partial E_i}{\partial B}$ for $i=1-3$ are calculated (Table II).

est focuses on explaining the variations in electronic properties in terms of changes in local structure in the MnX_4^{2-} tetrahedron: point symmetry and *X*-Mn bond distances. Furthermore we investigate whether pressure is able to induce aggregation processes among MnX_4^{2-} and $(CH_3)_4N^+$ tetrahedra yielding exchange-coupled phases involving Mn^{2+} with eventual changes in coordination. We have performed high-pressure experiments in single crystals of the two title compounds using time-resolved excitation and emission spectroscopy together with lifetime measurements in the 0–15 GPa range.

II. EXPERIMENTAL

Single crystals of $[(CH_3)_4N]_2MnCl_4$ and $[(CH_3)_4N]_2MnBr_4$ were grown by slow evaporation at 30 °C from HCl (or HBr) acidic solution containing a 2:1 stoichiometric ratio of the tetramethylammonium halide $[(CH_3)_4NX]$ and the corresponding metallic halide MnX_2.[8] The orthorhombic crystal structure, space group *Pmcn*, was checked by x-ray diffraction (XRD) using a Bruker D8 Advance diffractometer: $a=9.07$ Å; $b=15.66$ Å; and $c=12.33$ Å for $[(CH_3)_4N]_2MnCl_4$; and $a=9.23$ Å; $b=15.93$ Å; and $c=12.63$ Å for $[(CH_3)_4N]_2MnBr_4$.[23] A similar procedure was employed to grow and structural characterize the hexagonal ($P6_3/m$ space group) trihalides $(CH_3)_4NMnCl_3$ and $(CH_3)_4NMnBr_3$ (1:1 stoichiometric ratio). Besides x-ray diffraction, the biaxial and uniaxial character of the tetrahalides and trihalides, respectively, was checked with a polarizing microscope through their characteristic conoscopic images. The absorption spectra at ambient conditions were obtained with a Cary 6000i spectrophotometer. Pressure experiments were performed on a membrane-type DAC. The DAC was loaded with a suitable single crystal ($100\times80\times20$ μm^3) of either $[(CH_3)_4N]_2MnCl_4$ or $[(CH_3)_4N]_2MnBr_4$, and ruby spheres (<10 μm diameter) using silicone oil (Dow Corning 200 fluid 300000 cst) as pressure transmitting medium. The pressure was calibrated from the ruby PL *R*-line shift. The ruby PL and the emission spectra of the title compounds under high-pressure conditions were primarily obtained using a cw Kr^+ Coherent Innova I-300 laser and a double monochromator (Jobin-Yvon, Ramanor U1000). Time-resolved emission and excitation spectra in the 410–900 nm range were obtained using a Vibrant B 355 II OPO laser as tunable excitation light. The excitation light was focused backward on the sample with a 20× microscope objective, and the PL light was collected upward with another 20× objective and dispersed by a 0.5 m monochromator (Chromex 500IS). A Hamamatsu R928-S photomultiplier was employed for light detection using photon-counting techniques (SR 400). For lifetime measurements, the PL decay signal was detected with a Tektronix 2430 scope using suitable interference filters. Figure 4 shows a modification of the experimental setup described elsewhere,[24] for time-resolved spectroscopy.

III. RESULTS AND DISCUSSION

A. Emission–excitation spectra and photoluminescence lifetime of $[(CH_3)_4N]_2MnCl_4$ and $[(CH_3)_4N]_2MnBr_4$ at ambient conditions

Figures 1 and 2 show the absorption and associated emission spectra of $[(CH_3)_4N]_2MnX_4$ and $(CH_3)_4NMnX_3$ (*X*: Cl, Br) at ambient conditions. The absorption peaks correspond to electronic transition from the $^6A_1$ ground state of Mn^{2+} to different excited states of $MnX_4^{2-}(T_d)$ in $[(CH_3)_4N]_2MnX_4$ and the $MnX_6^{2-}(O_h)$ in $(CH_3)_4NMnX_3$. The peaks are assigned to tetrahedral or octahedral crystal-field transitions according to the corresponding irreps (in T_d- or O_h- symmetry notation).[14] Their excitation energies can be explained on the basis of crystal-field models through the Tanabe-Sugano (TS)

TABLE I. Experimental transition energy taken at the band maximum from the optical absorption and emission spectra at T=290 K (Figs. 1 and 2), and calculated energies for Mn^{2+} in T_d and O_h symmetries. The calculated energies were obtained by fitting the experimental energies to the energy terms of a d^5 electron configuration. The fit Racah parameters *B* and *C*, and crystal-field splitting, Δ are collected together with the standard deviation σ.[14–17] The Trees and Seniority parameters for Mn^{2+} were kept fixed: α=0.0081 eV (65 cm^{-1}) and Q=−0.0162 eV (−131 cm^{-1}) (Ref. 17). The PL energy and the corresponding Stokes shift for each compound are also included. Note that the smaller *B* and Δ values obtained for $[(CH_3)_4N]_2MnBr_4$ in comparison to $[(CH_3)_4N]_2MnCl_4$ reflect the increase in covalence and bond distance on passing from Mn-Cl to Mn-Br. Note also the increases in Δ on passing from $[(CH_3)_4N]_2MnX_4$ to $(CH_3)_4NMnX_3$(*X*:C1,Br), responsible for the green to red PL change. The corresponding C/B ration decreases from 5 to 4.

	$[(CH_3)_4N]_2MnCl_4$		$(CH_3)_4NMnCl_3$	
Excitation band assignment (T_d/O_h)	Observed (eV)	Calculated (eV)	Observed (eV)	Calculated (eV)
$^6A_1(S)\rightarrow{}^4T_1(G)$	2.65	2.62	2.33	2.34
$\rightarrow{}^4T_2(G)$	2.77	2.83	2.79	2.77
$\rightarrow{}^4A_1,\ {}^4E(G)$	2.87	2.88	2.95	2.96
$\rightarrow{}^4T_2(D)$	3.26	3.27	3.35	3.33
$\rightarrow{}^4E(D)$	3.38	3.35	3.48	3.50
$\rightarrow{}^4T_1(P)$	3.46	3.45	3.79	3.79
$\rightarrow{}^4A_2(F)$		4.53		4.77
$\rightarrow{}^4T_1(F)$		4.56		4.82
$\rightarrow{}^4T_2(F)$		4.65		5.09
Emission $^4T_1\rightarrow{}^6A_1$	2.38		1.98	
Stokes shift $^4T_1\leftrightarrow{}^6A_1$	0.27		0.35	
B		0.082		0.093
C		0.381		0.373
C/B		4.7		4.0
Δ		0.421		0.802
σ	0.033		0.016	
	$[(CH_3)_4N]_2MnBr_4$		$(CH_3)_4NMnBr_3$	
Excitation band assignment (T_d/O_h)	Observed (eV)	Calculated (eV)	Observed (eV)	Calculated (eV)
$^6A_1(S)\rightarrow{}^4T_1(G)$	2.64	2.61	2.33	2.32
$\rightarrow{}^4T_2(G)$	2.74	2.80	2.76	2.75
$\rightarrow{}^4A_1,\ {}^4E(G)$	2.84	2.84	2.88	2.93
$\rightarrow{}^4T_2(D)$	3.21	3.21	3.32	3.31
$\rightarrow{}^4E(D)$	3.30	3.28	3.48	3.48
$\rightarrow{}^4T_1(P)$	3.42	3.41	3.73	3.71
$\rightarrow{}^4A_2(F)$		4.45		4.45
$\rightarrow{}^4T_1(F)$		4.47		4.77
$\rightarrow{}^4T_2(F)$		4.56		5.04
Emission $^4T_1\rightarrow{}^6A_1$	2.37		1.95	
Stokes shift $^4T_1\leftrightarrow{}^6A_1$	0.27		0.38	
B		0.078		0.095
C		0.381		0.363
C/B		4.9		3.8
Δ		0.398		0.772
σ	0.029		0.020	

diagrams.[14,15] The TS diagram of Fig. 3 has been calculated as a function of crystal-field energy (Δ) in T_d and O_h symmetries using the Racah parameters *B* and *C* obtained by fitting the experimental energies obtained from the absorp-

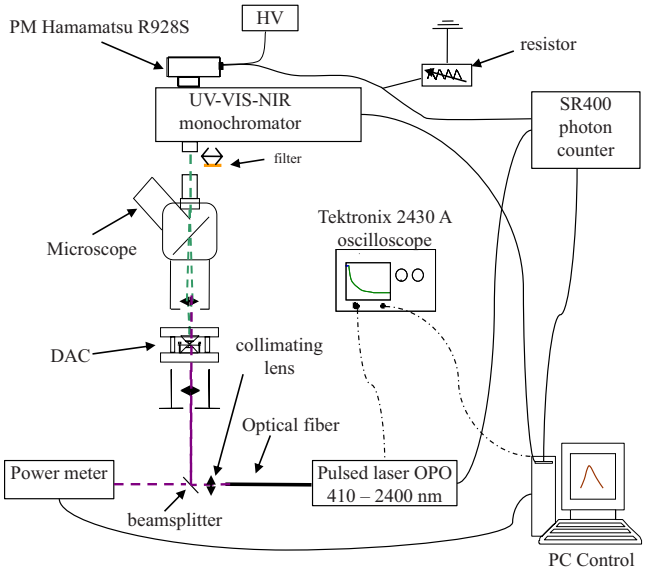

FIG. 4. (Color online) Experimental setup for time-resolved excitation and emission spectroscopy under high pressure conditions using diamond anvil cells. For lifetime measurements, the PL decay curve was detected by means of an oscilloscope using adequate load resistors. The excitation spectrum was corrected by normalizing the emission signal to the average energy of the excitation pulses for each wavelength using a power meter. Time delays and photon-counting times were selected and programmed in the SR400 photon counter according to the excited state dynamics of the emitting state.

tion (or excitation) spectra.[14,15] The observed and calculated energies for $[(CH_3)_4N]_2MnX_4$ and $(CH_3)_4NMnX_3$ (X:Cl,Br) at ambient conditions are collected in Table I, together with the corresponding B, C, and Δ parameters derived by fitting from the optical spectra of $[(CH_3)_4N]_2MnX_4$, orthorhombic $Pmcn$ (Refs. 25 and 26) and $(CH_3)_4NMnX_3$, hexagonal $P6_3/m$,[27] for X: Cl and Br.

It must be noted the drastic change in PL behavior on passing from $[(CH_3)_4N]_2MnX_4$ to $(CH_3)_4NMnX_3$. As shown in Fig. 2, the green emission of the $[(CH_3)_4N]_2MnX_4$ compounds appears in the same spectral region; its maximum being observed at 2.38 eV (521 nm) for X: Cl and 2.37 eV (523 nm) for X: Br. The origin of the green PL in comparison to the red emission of sixfold coordinated Mn^{2+} peaking at 1.98 eV (626 nm) (Fig. 1) and 1.95 eV (636 nm)[13,20] for $(CH_3)_4NMnCl_3$ and $(CH_3)_4NMnBr_3$, respectively, is caused by the weaker crystal field attained in $MnX_4^{2-}(T_d)$ with respect to $MnX_6^{4-}(O_h)$ (Fig. 3 and Table I). In particular, the crystal-field splitting for $MnCl_4^{2-}$ is $\Delta=0.4$ eV whereas $\Delta=0.8$ eV for $MnCl_6^{4-}$.[17,28–30] According to Figs. 1 and 3, this difference in Δ is responsible for the green emission at 2.38 eV and the red emission at 1.98 eV, the energy difference of which basically coincides with the crystal-field splitting difference exhibited by the tetra- and trihalides, respectively: $\delta\Delta=\Delta(O_h)-\Delta(T_d)=0.4$ eV. The TS diagram of Fig. 3 illustrates this behavior. As $\Delta(O_h)$ is twice $\Delta(T_d)$, the first $^4T_1$ emitting excited state in T_d lies 0.4 eV above the $^4T_{1g}$ in O_h thus yielding green and red PL, respectively. The crystal-field parameters obtained for $MnCl_4^{2-}$ and $MnBr_4^{2-}$ are fairly similar (Table I). Their main differences can be accounted for by slight differences of B and Δ attained in $MnBr_4^{2-}$ ($B=0.078$ eV; $\Delta=0.40$ eV) as consequence of the larger covalency of the Mn-Br bond in comparison to Mn-Cl ($B=0.082$ eV; $\Delta=0.42$ eV for $MnCl_4^{2-}$) and the faintly longer bond length: 2.48 Å for Mn-Br[27] and 2.34 Å Mn-Cl.[25] The higher covalency of tetrahalides with respect to trihalides is clearly evidenced by the slightly redshift of the Δ-independent $^4A_1\,{}^4E$ peak, whose transition energy only depends on B and C, and has values of 2.87 eV for $[(CH_3)_4N]_2MnCl_4$ and 2.95 eV for $(CH_3)_4NMnCl_3$. The C/B ratio also decreases on passing from T_d ($C/B\approx5$) to O_h ($C/B\approx4$). However, this variation is mainly due to the larger variation in B with respect to C. It must be noted that the PL Stokes shift between the first $^6A_1\rightarrow{}^4T_1$ excitation and the corresponding $^4T_1\rightarrow{}^6A_1$ emission, $E_{SS}=E_1-E_{PL}$, increases significantly on passing from T_d to O_h. This well-known result is associated with the increase in $A=\frac{\partial E(^4T_1-{}^6A_1)}{\partial\Delta}=\frac{\partial E_1}{\partial\Delta}$ upon increasing Δ as is observed in the TS diagram of Fig. 3. The slope A is directly related to the linear electron-lattice coupling hence to the Huang-Rhys factor by $S\propto\frac{A^2}{\omega^3}$.[18,31,32] Therefore the Stokes shift, which is related to A and the frequency of the coupled mode (ω) through the expression: $E_{SS}=2S\hbar\omega\propto(\frac{A}{\omega})^2$,[18,22,31,32] should increase with A, provided that ω varies less significant than A. The increase in E_{SS} from 0.27 eV in $[(CH_3)_4N]_2MnCl_4$ to 0.35 eV in $(CH_3)_4NMnCl_3$ must be ascribed to the increase in A from −0.83 for $\Delta=0.4$ eV ($MnCl_4^{2-}$) to −0.96 for $\Delta=0.8$ eV ($MnCl_6^{4-}$) (Tables I and II, and Fig. 3), given that the corresponding frequency of the a_{1g} coupled mode changes only from 32.0 meV (258 cm^{-1}) (Refs. 2 and 33) to 31.2 meV (252 cm^{-1}),[11,34] respectively. Therefore the measured Stokes

TABLE II. Experimental pressure derivatives of the excitation and emission energies, $\frac{\partial E_i}{\partial P}$ for $i=1-3$, for $Mn^{2+}(T_d)$ in the 0–10 GPa range in $[(CH_3)_4N]_2MnBr_4$ and $[(CH_3)_4N]_2MnCl_4$ (Fig. 7). The calculated pressure derivatives $\frac{\partial\Delta}{\partial P}$ and $\frac{\partial B}{\partial P}$ derived from the Tanabe-Sugano diagrams of Fig. 3 are also included.

Energy derivative[a]		$[(CH_3)_4N]_2MnCl_4$	$[(CH_3)_4N]_2MnBr_4$
Experimental	$\partial E_3/\partial P$	−12.3	−20.5
	$\partial E_2/\partial P$	−14.6	−23.4
	$\partial E_1/\partial P$	−18.6	−31.1
	$\partial E_{em}/\partial P$	−13.9	−23.4
	$\partial E_{SS}/\partial P$	−4.7	−7.7
Calculated Tanabe-Sugano Diagrams[b]	$\partial E_1/\partial\Delta$	−0.83	
	$\partial E_2/\partial\Delta$	−0.23	
	$\partial E_3/\partial\Delta$	0	
	$\partial E_1/\partial B$	−37	
	$\partial E_2/\partial B$	−36	
	$\partial E_3/\partial B$	−35	
	$\partial B/\partial P$	−0.35	−0.60
	$\partial\Delta/\partial P$	8	13

[a]Energy derivatives as a function of the pressure are in meV/GPa
[b]$C/B=5$ and $B=0.078$ eV for $\partial E/\partial\Delta$; and $\Delta=0.415$ eV for $\partial E/\partial B$.

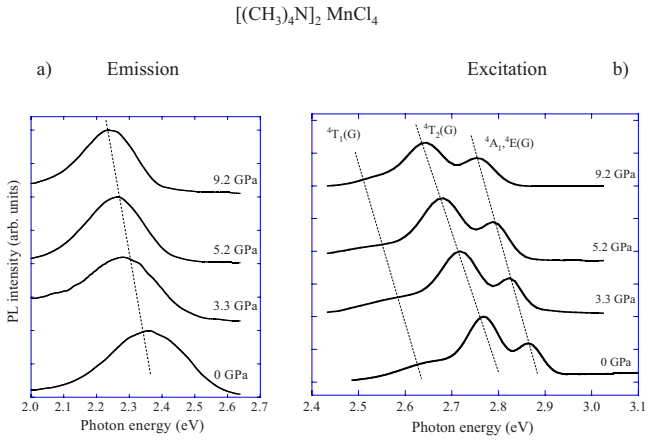

FIG. 5. (Color online) (a) Variation in the emission spectrum and (b) corresponding excitation spectrum of $[(CH_3)_4N]_2MnCl_4$ with pressure in upstroke. The excitation spectra were obtained by detecting the emission light at 2.39 eV (540 nm) for 300 μs after the excitation pulse of an OPO laser. The average counting was 100. The emission spectra were obtained upon excitation in 2.64 eV (470 nm) using the same photon-counting parameters employed for the excitation spectra.

shift ratio, $r_{SS}=\frac{E_{SS}(MnCl_4^{2-})}{E_{SS}(MnCl_6^{4-})}=\frac{0.27}{0.35}=0.77$, fairly correlates with the square ratio of corresponding slopes, $r_A=(\frac{-0.83}{-0.96})^2=0.75$. A similar situation occurs for the isomorphous bromides. The present analysis of the PL Stokes shift is worthy on discussing pressure effects in the optical spectra.

B. Pressure effects on MnX_4

Figures 5 and 6 show the variation in the emission and corresponding excitation spectra of $[(CH_3)_4N]_2MnCl_4$ and $[(CH_3)_4N]_2MnBr_4$ with pressure at room temperature. Due to

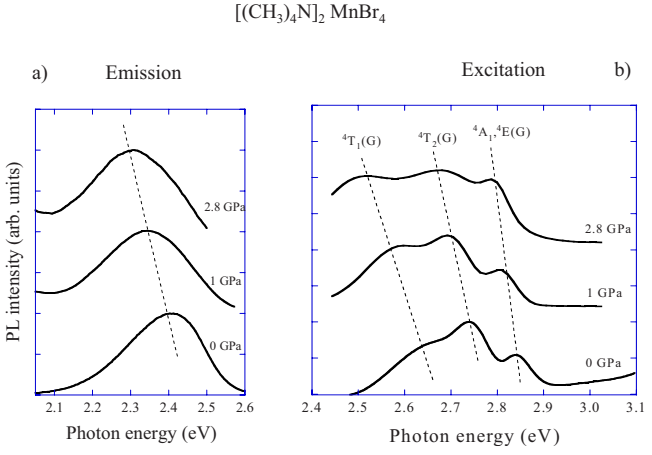

FIG. 6. (Color online) (a) Variation in the emission spectrum and (b) corresponding excitation spectrum of $[(CH_3)_4N]_2MnBr_4$ with pressure in upstroke. The excitation spectra were obtained by detecting the emission light at 2.39 eV (540 nm) for 300 μs after the excitation pulse of an OPO laser. The average counting was 100. The emission spectra were obtained upon excitation at 2.64 eV (470 nm) using the same photon-counting parameters employed for the excitation spectra.

instrumental limitations imposed by the OPO laser, excitation spectra contain the first three crystal-field peaks, named E_1, E_2, and E_3, which are related to the $Mn^{2+}(T_d)$ transitions $^6A_1 \rightarrow {}^4T_1$, $^4T_2$, $^4A_1$ ^4E, respectively. At ambient pressure, the peak energies are located at $E_1=2.65$ eV, $E_2=2.77$ eV and $E_3=2.86$ eV in $[(CH_3)_4N]_2MnCl_4$, and 2.64, 2.74, and 2.85 eV, respectively, in $[(CH_3)_4N]_2MnBr_4$. Figure 7 shows the variation in the excitation and emission energies with pressure obtained from the excitation spectra of $[(CH_3)_4N]_2MnX_4$ $(X:Cl,Br)$ and the corresponding least-square linear fit equations. The experimental peak energies were obtained by fitting each excitation spectrum to three Gaussian bands taking the fitted parameters of each ambient-pressure spectrum as initial parameters to fit the spectra at higher pressures. Along with the fit, both width and intensity of the three bands were kept in a limited range in order to preserve the physical significance of the fitting according to the spectral shape. The experimental data of Fig. 7 correspond to the fitted energies following this procedure, and the linear equations, $E_i(P)$ for i=1–3, are the least-square fit to experimental data.

It is worth noting that the energies of the emission and the three excitation peaks shift to lower energies with pressure following a linear behavior with similar slopes for each compound (Fig. 7; Table II). This behavior contrasts with the TS-diagram trends foreseeing a weak pressure dependence of the Δ-independent E_3 with respect to the Δ-dependent E_1 and E_2, provided that pressure mainly increases Δ. The fact the three $E_i(P)$ variations run almost parallel with pressure clearly indicates that the variations in B and C with pressure are more important than the variations in Δ in order to account for the observed shift rates. In particular, three relevant features must be underlined: (1) the three excitation energies E_1, E_2, and E_3 decrease linearly with pressure, their shift rates being $-18.6(^4T_1)$, $-14.6(^4T_2)$ and $-12.3(^4A_1\ ^4E)$ meV/GPa, which are similar to the emission rate of -13.9 meV/GPa in $[(CH_3)_4N]_2MnCl_4$; the corresponding shift rates in $[(CH_3)_4N]_2MnBr_4$ are $-31.1(^4T_1)$, $-23.4(^4T_2)$ and $-20.5(^4A_1\ ^4E)$ meV/GPa for excitation and -23.4 meV/GPa for emission; (2) the pressure-induced redshift of the excitation energies runs nearly parallel to the emission redshift thus indicating reduction of B and C rather than increase in Δ; (3) the variation in the excitation and emission spectra with pressure (Figs. 5 and 6), and their corresponding peak-energy variations (Fig. 7), show no evidence of pressure-induced local distortions around Mn^{2+} beyond T_d symmetry. For example, a hypothetical low-symmetry distortion of D_{2d} symmetry in MnX_4^{2-} would split the $^4T_{1,2}$ manifold in two states $[^4E+(^4A_2,\ ^4B_2)]$ leading to a bigger PL pressure shift in comparison to the corresponding excitation redshift.[16,17] Therefore we conclude that pressure induces redshifts in both emission and excitation peaks but keeping the T_d symmetry of MnX_4^{2-}.

The slopes of $E_i(P)$ confirm that pressure-induced peak shifts are first governed by a reduction of B and C, and second by an increase in Δ due to shortening of the Mn-X bond, i.e., increase in Mn-X bond covalency and Δ, respectively. Pressure-induced shifts can be described in terms of B, C and Δ through the equation:

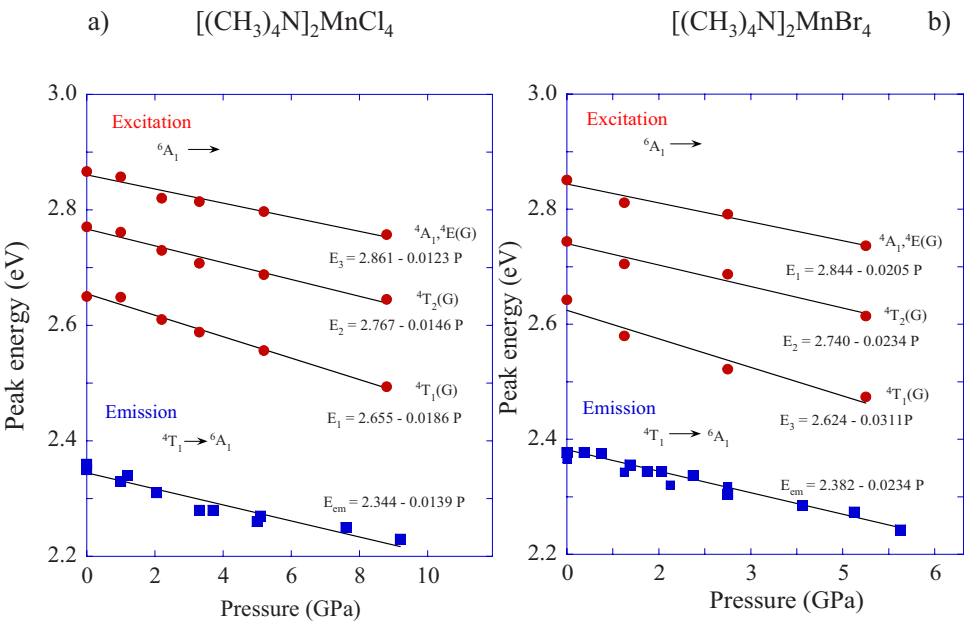

FIG. 7. (Color online) Experimental variation in the excitation and emission energies with pressure for (a) $[(CH_3)_4N]_2MnCl_4$ and (b) $[(CH_3)_4N]_2MnBr_4$. The least-square linear fit equations are included for the three excitation and the emission peaks.

$$\left(\frac{\partial E_i}{\partial P}\right)_{P_0} = \left(\frac{\partial E_i}{\partial B}\right)\frac{\partial B}{\partial P} + \left(\frac{\partial E_i}{\partial C}\right)\frac{\partial C}{\partial P} + \left(\frac{\partial E_i}{\partial \Delta}\right)\frac{\partial \Delta}{\partial P}$$

$$= [A_i + (C/B)D_i]\frac{\partial B}{\partial P} + \left(\frac{\partial E_i}{\partial \Delta}\right)\frac{\partial \Delta}{\partial P} \quad (1)$$

For a given C/B ratio, A_i and D_i are the coefficients of the Racah parameter (B, C) for E_i, and i stands for the three peak energies, $i=1-3$.[14,15] Quantitative estimates of these two effects can be obtained from the experimental peak shifts and the slopes $\partial E_i/\partial\Delta$ or $\partial E_i/\partial B$ $(i=1-3)$ derived from the TS diagrams of Fig. 3. We know that the $^4A_1\ ^4E$ energy (E_3) does not depend on Δ but B or C $(\partial E_3/\partial\Delta = 0)$. It means that its pressure dependence can be written for C/B=5 as:

$$\frac{\partial E_3}{\partial P} = 10\frac{\partial B}{\partial P} + 5\frac{\partial C}{\partial P} = 35\frac{\partial B}{\partial P} \quad (2)$$

However both $^4T_1$ and $^4T_2$ energies (E_1 and E_2, respectively) depend on B, C, and Δ, and their slope can be derived from the TS diagram as well (Table II). So that the energy variations with pressure can be expressed as follows:

$$\frac{\partial E_{1,2}}{\partial P} = \left(\frac{\partial E_{1,2}}{\partial B}\right)_\Delta \frac{\partial B}{\partial P} + \left(\frac{\partial E_{1,2}}{\partial \Delta}\right)_{B,C}\frac{\partial \Delta}{\partial P}$$

$$\approx 35\frac{\partial B}{\partial P} + \left(\frac{\partial E_{1,2}}{\partial \Delta}\right)_{B,C}\frac{\partial \Delta}{\partial P} \quad (3)$$

or likewise

$$\frac{\partial (E_{1,2} - E_3)}{\partial P} \approx \left(\frac{\partial E_{1,2}}{\partial \Delta}\right)_{B,C}\frac{\partial \Delta}{\partial P}. \quad (4)$$

The slopes $(\partial E_{1,2}/\partial\Delta)_{B,C}$ or $(\partial E_{1,2}/\partial B)_\Delta$ have been obtained from the TS diagrams of Fig. 3 that we calculated as a function of Δ for fixed values of B and C, and as a function of B keeping C/B constant for a fixed value of Δ. These coefficients together with the experimental pressure coefficients for the three excitation peaks and their corresponding emission are collected in Table II. From Eqs. (2) and (4) we obtain $\partial B/\partial P = -0.35$ meV/GPa or $\partial\Delta/\partial P = +8.0$ meV/GPa for $[(CH_3)_4N]_2MnCl_4$; or $\partial B/\partial P = -0.60$ meV/GPa or $\partial\Delta/\partial P = +13.0$ meV/GPa for $[(CH_3)_4N]_2MnBr_4$. Although $\partial\Delta/\partial P$ for T_d is about four times smaller than in O_h, the values of $\partial B/\partial P$ are in fairly agreement with those measured in sixfold coordinated systems as $MnCl_6^{4-}(O_h)$ in NH_4MnCl_3: $\partial B/\partial P = -0.3$ meV/GPa or $\partial\Delta/\partial P = +35$ meV/GPa [14,35] and also in $MnCl_2$ ($\partial B/\partial P = -0.3$ meV/GPa; $\partial\Delta/\partial P = +32$ meV/GPa) or $MnBr_2$ (−0.45 and +37 meV/GPa, respectively).[36] In $CsZnX_4$:Co^{2+} where the Co^{2+} occupies the substitutional $Zn(T_d)$ site as CoX_4^{2-}, these variations are: $\partial B/\partial P = -0.7$ or −0.8 meV/GPa; $\partial\Delta/\partial P = 9$ and 8 meV/GPa for X: Cl and Br, respectively,[37] which are similar to those found in MnX_4^{2-}. Although $[(CH_3)_4N]_2MnCl_4$ is more compressible than NH_4MnCl_3,[35] it is worth noting that the variation in B is similar for both crystals but Δ varies three times bigger in the perovskite. These results suggest that the local compressibility of MnX_4^{2-} is smaller than the crystal compressibility. The stiffness of Mn-X bonds in comparison to hydrogen bonds governing the crystal compressibility is probably responsible for such difference. Nevertheless the covalence in $MnX_4^{2-}(T_d)$, measured through B, has a stronger pressure dependence than in $MnX_6^{4-}(O_h)$. At variance with sixfold coordinate Mn^{2+}, the main contribution to the pressure-induced redshift in MnX_4^{2-} is reduction of B and C (covalence effect) rather than increase in Δ. In fact, the covalency contribution to the redshift is given by $35\partial B/\partial P = -12$ meV/GPa for X: Cl (−20 meV/GPa for X: Br) whereas the crystal-field contribution is $\partial\Delta/\partial P = 8$ meV/GPa for X: Cl (13 meV/GPa for X: Br), and thus each contribution represents about 2/3 and 1/3 of the total redshift, respectively. It is worth noting that

the unexpectedly weak contribution of the crystal-field to the pressure-induced peak shift must be ascribed to the small values of Δ in fourfold T_d systems in comparison to sixfold O_h. The strong covalence effect attained in T_d systems has also important consequences in the pressure shifts of CoX_4^{2-} formed in different systems as Cs_2CoCl_4, Cs_2CoBr_4, ZnO and ZnS.[37] The present results on $Mn^{2+}(T_d)$ are worthy to explain the intricate behavior of $Co^{2+}(T_d)$ systems under high-pressure conditions.

Interestingly, the reduction of Mn-X distance with pressure can be estimated from the optical spectra through $\partial\Delta/\partial P$, on the assumption of a R dependence of Δ as R^{-5}.[3,32,35] Consequently, we can derive $\partial R_{\text{Mn-}X}/\partial P$ through the equation: $\frac{1}{\Delta}\frac{\partial\Delta}{\partial P}=\frac{-5}{R_{\text{Mn-}X}}\frac{\partial R_{\text{Mn-}X}}{\partial P}$. Taking $\Delta=0.398$ eV and $R_{\text{Mn-Br}}=2.48$ Å, we obtain $\frac{\partial R_{\text{Mn-Br}}}{\partial P}=-\frac{1}{5}\frac{R_{\text{Mn-Br}}}{\Delta}\frac{\partial\Delta}{\partial P}=-\frac{1}{5}\times\frac{2.48}{0.398}\times 0.013=-0.016$ Å/GPa. It means a local bulk modulus for $MnBr_4^{2-}$ in $[(CH_3)_4N]_2MnBr_4$, $B_{\text{loc}}=-V_{\text{loc}}\frac{\partial P}{\partial V_{\text{loc}}}=-\frac{R_{\text{Mn-Br}}}{3}\frac{\partial P}{\partial R_{\text{Mn-Br}}}=52$ GPa. This estimate reveals that the local $MnBr_4^{2-}$ compressibility would be significantly smaller (by a factor 5) than the crystal compressibility. Analogously, we obtain $B_{\text{loc}}=87$ GPa for $MnCl_4^{2-}$ in $[(CH_3)_4N]_2MnCl_4$ taking $\Delta=0.421$ eV, $R_{\text{Mn-Cl}}=2.34$ Å, or $\partial R_{\text{Mn-Cl}}/\partial P=-0.009$ Å/GPa. These values are similar to local bulk modulii measured for $CuCl_6^{4-}$ ($B_{\text{loc}}=63$ GPa) in $(C_3H_7NH_3)_2CuCl_4$ using both x-ray absorption (XAS) and XRD under high-pressure conditions.[38]

The Stokes shift decreases with pressure by −4.7 and −7.7 meV/GPa in $[(CH_3)_4N]_2MnCl_4$ and $[(CH_3)_4N]_2MnBr_4$, respectively. Such a shift rate was obtained from the linear dependence of E_{SS} with pressure as $E_{SS}(\text{eV})=0.27-0.0047$ P(GPa) and $E_{SS}(\text{eV})=0.27-0.0077$ P(GPa), respectively. This behavior is similar to findings in sixfold MnX_6^{4-} along the Mn^{2+}-doped perovskite series $ABX_3:Mn^{2+}$ (X: Cl, F),[18,28] and reflects the hardening of the vibrational coupled mode, ω, with respect to the electron-phonon coupling A. Given that the pressure derivatives of the $^6A_1\rightarrow{}^4T_1$ energy in MnX_4^{2-} is three times smaller than in MnX_6^{4-}, the Stokes-shift reduction by pressure is more effective in $Mn^{2+}(T_d)$ as is experimentally demonstrated in the present work.

C. Pressure-induced structural transformation: change in coordination $MnX_4\leftrightarrow MnX_6$

The emission spectra of $[(CH_3)_4N]_2MnCl_4$ and $[(CH_3)_4N]_2MnBr_4$ change drastically above 12 and 5 GPa, respectively (Fig. 8). The single redshifted green emission, which is characteristic of the $MnX_4^{2-}(T_d)$, transforms to an inhomogeneously broadened green/red multiband emission over the 500–800 nm range above these pressures, whose associated lifetime is wavelength dependent. Figure 8 shows the variation in the emission spectra upon pressure release from the high-pressure phase. It must be noted that the PL spectrum back transforms into a double band emission peaking at 2.3 eV (green-yellow emission 550 nm) and 1.8 eV (red emission 650 nm). Although the two bands and their energy have been observed in different experiments and depend on pressure, their relative intensity however is sample dependent and, for a given sample, varies upon excitation in different zones of the pressurized single crystal. Furthermore, the two-color emissions induced by pressure release undergo noticeable redshifts producing a marked piezo-PL effect (Fig. 8). The observation of the two emissions down to 1 GPa is noteworthy. It means that the associated Mn^{2+} phases responsible for each emission coexist in a wide pressure range near ambient pressure. At zero pressure the emission spectrum recovers the single green emission of $MnX_4^{2-}(T_d)$ in $[(CH_3)_4N]_2MnX_4$. The large pressure range of phase coexistence observed in downstroke foresees these materials as a type of multiband PL behavior, whose properties can be tuned through pressure and eventually stabilized at ambient conditions. The lack of complete recovery of the PL lifetime, τ(P), at zero pressure in downstroke may be caused by slightly residual stresses in the pressure cavity.

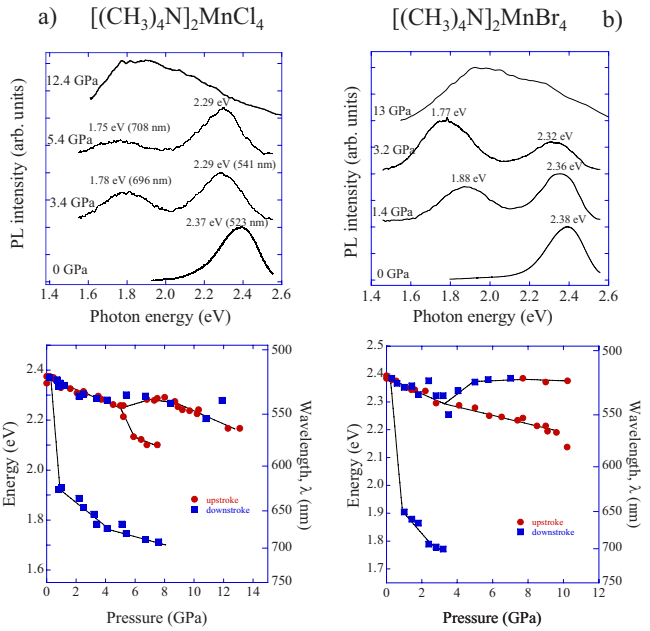

FIG. 8. (Color online) Pressure-dependence of the emission spectra of (a) $[(CH_3)_4N]_2MnCl_4$ and (b) $[(CH_3)_4N]_2MnBr_4$ in downstroke starting from 12 and 6 GPa, respectively. The emission spectra were obtained by detecting upon excitation with an OPO pulsed light of 470 nm for 300 μs after the excitation pulse. The average counting was 100 spectra. The variation in the emission energy at the band maxima and corresponding wavelength are included below. Note the large redshifts exhibited by the red emission with pressure as well as the pressure hysteresis along the process.

These experiments suggest that pressure induces aggregation processes between $MnX_4^{2-}(T_d)$ yielding Mn^{2+} phases coexisting in a wide pressure range. The pressure dependence of τ(P), shown in Fig. 9, supports this view. The reason is the following: $(CH_3)_4NMnCl_3$ and $(CH_3)_4NMnBr_3$ have PL lifetimes of 800 μs [39,40] and 500 μs,[40,41] respectively, at ambient conditions. Like in most concentrated materials these decay lifetimes are fully governed by the exchange mechanism.[13,17,40,41] With the exception of the abrupt increase in τ in $[(CH_3)_4N]_2MnX_4$ from 0.9 to 3.5 ms at 0.5 GPa,[42] τ(P) continuously decreases with pressure in both crystals. This lifetime decrease is contrary to the increase

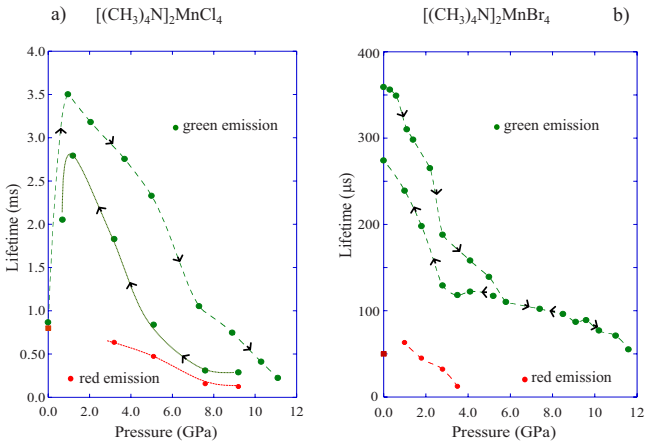

FIG. 9. (Color online) Variation in the PL lifetime τ(P) with pressure for the green and red emissions in (a) $[(CH_3)_4N]_2MnCl_4$ and (b) $[(CH_3)_4N]_2MnBr_4$. Lifetime data for each emission were derived from the single exponential decay curve $I_{exp}(t)$ measured as a function of pressure for the red and green emissions at 650 nm (red) and 540 nm (green), respectively. The experimental $I_{exp}(t)$ curves were fitted to the equation $I_{exp}(t)=I_0\exp(-t/\tau)+I_{bg}$. The background intensity I_{bg} was measured from $I_{exp}(t)$ at times before the excitation pulse. The red points at zero pressure represent the PL lifetime values of $(CH_3)_4NMnCl_3$ and $(CH_3)_4NMnBr_3$ at ambient conditions.

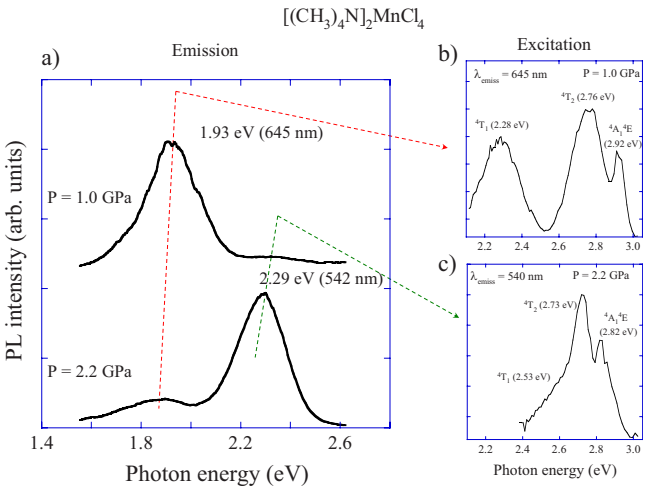

FIG. 10. (Color online) (a) Emission spectra of $[(CH_3)_4N]_2MnCl_4$ obtained in downstroke at 1.0 and 2.2 GPa by excitation with an OPO pulsed light of 470 nm for 400 μs and 3 ms, respectively, after the excitation pulse. (b) and (c) Excitation spectra corresponding to the green emission at 540 nm and the red emission at 645 nm, respectively. The crystal was excited with an OPO laser as a function of the excitation wavelength. The PL light intensity was detected by photon counting for 400 μs and 3 ms, respectively, after each excitation pulse. Spectra were corrected for excitation pulse energy and averaged for 100 spectra. Note the different excitation spectrum obtained for each emission (see Table I for comparison). Note also that the emission spectra shown at 1.0 and 2.2 GPa were obtained for counting times of 400 μs and 3 ms, respectively, in order to enhance the relative intensity of the red and green emissions according to their respective PL lifetimes.

observed in isolated Mn^{2+} (Refs. 16 and 22) as well as other isolated transition-metal ions under pressure such as Cr^{3+} in Al_2O_3 (ruby);[21,43] and Cr^{3+} in $LiCaAlF_6$ and Rb_2KCrF_6 (fluoroelpasolites);[44,45] or Ti^{3+} in Al_2O_3 (sapphire).[46] Therefore the observed decrease in τ(P) with pressure is not associated with nonradiative de-excitation processes within MnX_4^{2-} (Refs. 1–3) but can be probably associated with an increase in the Mn-Mn coupling interaction as a consequence of the progressive approach of Mn^{2+} ions with pressure. The similarity between PL lifetimes of red and green emissions at high pressure supports this interpretation. In fact, τ(P) decreases an order of magnitude in $[(CH_3)_4N]_2MnCl_4$ in the 0–10 GPa range while decreases a factor 4 in $[(CH_3)_4N]_2MnBr_4$ in the 0–6 GPa range (Fig. 9). In downstroke, τ(P) varies differently for the red and green emissions (Fig. 9). Its variation for the red emission is weaker than for the green emission. The extrapolated red-emission lifetime at zero pressure is 0.8 ms in both crystals. These values are comparable to the Mn^{2+} lifetime attained in the one-dimensional $(CH_3)_4NMnCl_3$ and $(CH_3)_4NMnBr_3$ with lifetimes of 800 μs (Ref. 39) and 500 μs (Ref. 41) at ambient conditions, respectively. Therefore we can reasonably ascribe red PL to sixfold coordinate Mn^{2+} (MnX_6^{4-}) formed by MnX_4^{2-} packing. Hence the formation of Mn^{2+} phases similar to $(CH_3)_4NMnX_3$ from pressure-induce decomposition of $[(CH_3)_4N]_2MnX_4$ is likely.

In order to reveal the microscopic origin of the two-color emission of Mn^{2+} in $[(CH_3)_4N]_2MnX_4$ under high-pressure conditions, we have performed time-resolved excitation spectroscopy in the green and red emissions. The results for $[(CH_3)_4N]_2MnCl_4$ are shown in Fig. 10. Similar results were obtained in $[(CH_3)_4N]_2MnBr_4$. The analysis of Figs. 8–10 shows that (i) both red and green emissions experience large redshifts with pressure, their relative intensity and corresponding lifetime being different. Note that the enhancement of the red emission with respect to the green emission at 1.0 GPa in contrast to the emission spectra taken at 2.2 GPa (Fig. 10) is due to the choice of parameters used in the time-resolve emission spectra. While at 1.0 GPa the counting gate was fixed at 3 ms, which is about the $MnCl_4^{2-}$ lifetime at this pressure, the gate was reduced to 400 μs at 2.2 GPa, thus favoring the emission of $MnCl_6^{4-}$ with respect to the longer lived $MnCl_4^{2-}$. (ii) the associated excitation spectrum is different for each emission, the spectral shape and transition energies clearly revealing which Mn^{2+} centers are responsible for each emission. By comparing the excitation spectra of Fig. 10 with the absorption spectra of Fig. 1 we conclude that the green emission corresponds to $MnCl_4^{2-}$, while the red emission is associated with $MnCl_6^{4-}$. The slight blueshift of the red-emission-related $^4A_1\,^4E$ excitation peak (2.92 eV) with respect to the green-emission-related $^4A_1\,^4E$ excitation peak (2.82 eV) and, particularly, the different position of the first $^4T_1$ excitation peak, 2.28 and 2.53 eV for red and green emissions, respectively, clearly support this interpretation. (iii) The resemblance between the excitation spectrum of $MnCl_6^{4-}$ and the absorption spectrum of $(CH_3)_4NMnCl_3$ (Fig. 1) suggests that pressure induces decomposition or solid-state reactions within $[(CH_3)_4N]_2MnCl_4$ leading to partial formation of either $(CH_3)_4NMnCl_3$ with linear chains of face-sharing $MnCl_6^{4-}$ or other mixed compounds such as

$[(CH_3)_3NH]_3Mn_2Cl_7$ having $MnCl_4^{2-}$ and $MnCl_6^{4-}$ centers simultaneously.[47] In either case we conclude that red and green emissions are not correlated and arise from differently coordinated Mn^{2+} centers, thus revealing formation of pressure-induced aggregated phases.

D. Structural model

Although a phase transition from $[(CH_3)_4N]_2MnCl_4$ to another sixfold-coordinate Mn^{2+} phase should not be ruled out *a priori*, the observation of an intense red PL in the high-pressure phase at room temperature, having a PL lifetime of 0.6 ms at 3.2 GPa discards any structure showing either three dimensional (3D) or two dimensional (2D) Mn^{2+} ordering. Besides one dimensional (1D), room-temperature PL is unlike in 2D and 3D Mn^{2+} structures due to exciton migration and subsequent transfer to nonradiative traps.[16–18] Hence, we consider that a 1D-Mn^{2+}-like structure or simpler dimer-like Mn-Mn systems are feasible high-pressure phases that could account for the red emission. Furthermore the excitation spectra show that green and red emissions come from different centers, the green corresponding to either $[(CH_3)_4N]_2MnCl_4$ or a distinct Mn^{2+} compound containing $MnCl_4^{2-}$ sites. A plausible scenario for explaining the unexpected PL behavior under high-pressure conditions envisages phase coexistence of 1D $(CH_3)_4NMnCl_3$ and 3D $[(CH_3)_4N]_2MnCl_4$. Pressure can induce solid-state reaction yielding decomposition $[(CH_3)_4N]_2MnCl_4 \rightarrow (CH_3)_4NMnCl_3 + (CH_3)_4NCl$. A similar scenario can also accounts for $[(CH_3)_4N]_2MnBr_4$. X-ray diffraction experiments under pressure aiming to elucidate whether a pressure induced phase transition or a chemical decomposition takes place in $[(CH_3)_4N]_2MnX_4$ (X=Cl, Br) are currently in progress. Interestingly, the large pressure range with two coexisting phases foresees these materials as attractive PL systems to eventually stabilize multiband emission at ambient conditions.

IV. CONCLUSIONS

The pressure dependence of the excitation and the emission spectra of tetrahedral MnX_4^{2-} formed in $[(CH_3)_4N]_2MnX_4$ (X=Cl, Br) shows that both the excitation and corresponding emission peaks shift to lower energy at similar rates (about −10 and −20 meV/GPa for chlorides and bromides, respectively). Crystal-field analysis reveals two main contributions to the redshift: reduction of the Racah parameters B and C, and increase in crystal-field Δ due to Mn-X shortening. At variance with sixfold coordinate MnX_6^{4-} centers, the main contribution to the pressure-induced redshift in MnX_4^{2-} is reduction of B and C (covalence effect), which represents 2/3 of the total redshift, rather than increase in Δ representing 1/3. On the other hand, the pressure dependence of the peak shift in MnX_6^{4-} (X: Cl, F) is mainly governed by variations in Δ rather than B and C. We show that the PL Stokes shift decreases with pressure in both crystals. We experimentally demonstrate that such behavior is due to the relatively weaker increase in the electron-phonon coupling than the hardening of the coupled vibration.

We have induced a two-color PL in $[(CH_3)_4N]_2MnX_4$ (X: Cl, Br) above 10 and 6 GPa, respectively. This phenomenon is interpreted in terms of chemical decomposition of $[(CH_3)_4N]_2MnX_4$ yielding at least two coexisting phases associated with MnX_4^{2-} (green emitter) and MnX_6^{4-} (red emitter) PL centers. The red emission arises from MnX_6^{4-}, whose structure probably corresponds to face-sharing MnX_6^{4-} octahedra like that attained in the 1D $(CH_3)_4NMnX_3$ structure.

ACKNOWLEDGMENTS

Financial support from the Spanish Ministerio de Ciencia e Innovación (Project No. MAT2008-06873-C02-01) and MALTA INGENIO-CONSOLIDER 2010 (Ref. No. CDS2007-0045) are acknowledged. Y. Rodriguez-Lazcano and L. Nataf thank financial support from the Mobility Program (Ref. No. SB2005-0201) and Postdoctoral fellowship from The University of Cantabria, respectively.

*Corresponding author; rodriguf@unican.es

[1] B. R. Sundheim, E. Levy, and B. Howard, J. Chem. Phys. **57**, 4492 (1972).
[2] M. T. Vala, C. J. Balhausen, R. Dingle, and S. L. Holt, Mol. Phys. **23**, 217 (1972).
[3] N. Presser, M. A. Ratner, and B. R. Sundheim, Chem. Phys. **31**, 281 (1978).
[4] G. E. Hardy and J. I. Zink, Inorg. Chem. **15**, 3061 (1976).
[5] B. P. Chandra and J. I. Zink, Phys. Rev. B **21**, 816 (1980).
[6] K. Nikolic, B. Canny, D. Curie, F. Gendrom, and C. Porte, Fizika (Zagreb) **1**, 27 (1985).
[7] M. C. Marco de Lucas and F. Rodriguez, J. Phys.: Condens. Matter **1**, 4251 (1989).
[8] M. C. Marco de Lucas and F. Rodriguez, J. Phys.: Condens. Matter **5**, 2625 (1993).
[9] F. A. Cotton, L. M. Daniels, and P. L. Huang, Inorg. Chem. **40**, 3576 (2001).
[10] B. P. Chandra, N. G. Deshmukh, R. B. Sahu, and A. K. Verma, Cryst. Res. Technol. **21**, 1559 (1986).
[11] K. E. Lawson, J. Chem. Phys. **47**, 3627 (1967).
[12] C. F. Putnik, G. M. Cole, and S. L. Holt, Inorg. Chem. **15**, 2135 (1976).
[13] R. A. Auerbach and G. L. McPherson, Phys. Rev. B **33**, 6815 (1986).
[14] J. S. Griffith, *The Theory of Transition-Metal Ions* (Cambridge University Press, Cambridge, England, 1980).
[15] S. Sugano, Y. Tanabe, and H. Kamimura, *Multiplets of Transition-Metal ions* (Academic Press, New York, 1970).
[16] I. Hernández, F. Rodríguez, and H. D. Hochheimer, Phys. Rev. Lett. **99**, 027403 (2007).
[17] I. Hernández and F. Rodriguez, J. Phys.: Condens. Matter **15**, 2183 (2003).
[18] B. Henderson and G. F. Imbusch, *Optical Spectroscopy of Inorganic Solids* (Oxford University Press, New York, 1989).

[19] A. Moral and F. Rodriguez, Rev. Sci. Instrum. **66**, 5178 (1995).
[20] J. I. Zink, G. E. Hardy, and G. Gliemann, Inorg. Chem. **19**, 488 (1980).
[21] K. Syassen, High Press. Res. **28**, 75 (2008).
[22] F. Rodríguez, I. Hernández, M. Moreno, and R. Alcalá, J. Chem. Phys. **119**, 8686 (2003).
[23] K. Gesi, J. Phys. Soc. Jpn. **52**, 2931 (1983).
[24] I. Hernandez, Ph.D. thesis, University of Cantabria, 2006.
[25] H. Mashiyama and N. Koshiji, Acta Crystallogr. B: Struct. Sci. **45**, 467 (1989).
[26] B. Morosin and E. J. Graeber, Acta Crystallogr. **23**, 766 (1967).
[27] K. Hasebe and T. Asahi, Acta Crystallogr. C: Cryst. Struct. Commun. **45**, 841 (1989).
[28] M. C. Marco de Lucas, F. Rodríguez, H. U. Güdel, and N. Furrer, J. Lumin. **60-61**, 581 (1994).
[29] M. C. Marco de Lucas, F. Rodríguez, C. Prieto, M. Verdaguer, M. Moreno, and H. U. Güdel, Radiat. Eff. Defects Solids **135**, 95 (1995).
[30] D. Hernández, F. Rodríguez, M. Moreno, and H. U. Güdel, Physica B **265**, 186 (1999).
[31] F. Rodríguez, P. Núñez, and M. C. Marco de Lucas, J. Solid State Chem. **110**, 370 (1994).
[32] M. C. Marco de Lucas, F. Rodríguez, and M. Moreno, Phys. Rev. B **50**, 2760 (1994).
[33] J. S. Avery, C. D. Burbridge, and D. M. L. Goodgame, Spectrochim. Acta [A] **24**, 1721 (1968).
[34] P. S. Peercy, B. Morosin, and G. A. Samara, Phys. Rev. B **8**, 3378 (1973).
[35] Variations of B, C and Δ as a function of P and R in NH_4MnCl_3 to be published.
[36] H. G. Drickamer and C. W. Frank, *Electronic Structure, Electronic Transitions and the High Pressure Chemistry and Physics of Solids* (Chapman and Hall, London, 1973).
[37] D. R. Stephens and H. G. Drickamer, J. Chem. Phys. **35**, 429 (1961).
[38] F. Rodríguez, F. Aguado, R. Valiente, M. Hanfland, and J. P. Itié, Phys. Status Solidi **244**, 156 (2007) b.
[39] C. Marco de Lucas and F. Rodríguez, Rev. Sci. Instrum. **61**, 23 (1990).
[40] M. Wrighton and D. Ginley, Chem. Phys. **4**, 295 (1974).
[41] W. J. Rodríguez, R. A. Auerbach, and G. L. McPherson, J. Chem. Phys. **85**, 6442 (1986).
[42] The origin of the sharp increase in lifetime in $[(CH_3)_4N]_2MnCl_4$ is caused by the strong dependence of the PL due to the activation of nonradiative processes at ambient conditions. A precise account of this phenomenon will be published in a forthcoming report.
[43] J. H. Eggert, K. A. Goettel, and I. F. Silvera, Phys. Rev. B **40**, 5733 (1989).
[44] I. Hernandez, F. Rodriguez, and A. Tressaud, Inorg. Chem. **47**, 10288 (2008).
[45] M. N. Sanz-Ortiz, F. Rodriguez, I. Hernandez, R. Valiente, and S. Kück, High Press. Res. **26**, 345 (2006).
[46] S. Garcia-Revilla, F. Rodriguez, R. Valiente, and M. Pollnau, J. Phys.: Condens. Matter **14**, 447 (2002).
[47] R. E. Caputo, S. Roberts, R. D. Willet, and B. C. Gerstein, Inorg. Chem. **15**, 820 (1976).